Chemical Engineering Journal 266 (2015) 156–162

Contents lists available at ScienceDirect

Chemical Engineering Journal

journal homepage: www.elsevier.com/locate/cej

Nanoparticle transport in saturated porous medium using magnetic resonance imaging

Susithra Lakshmanan [a,*], William M. Holmes [b], William T. Sloan [c], Vernon R. Phoenix [a]

[a] School of Geographical and Earth Sciences, Gregory Building, University of Glasgow, UK
[b] GEMRIC, Institute of Neuroscience and Psychology, University of Glasgow, UK
[c] School of Engineering, Rankine Building, University of Glasgow, UK

HIGHLIGHTS

- Carboxyl-functionalized nanoparticle through sandstone rock core was studied.
- MR imaging technique was used to image the NP transport.
- Transport parameters were estimated using CXTFIT computer package.
- Nanoparticle–surface interactions were investigated using DLVO.

GRAPHICAL ABSTRACT

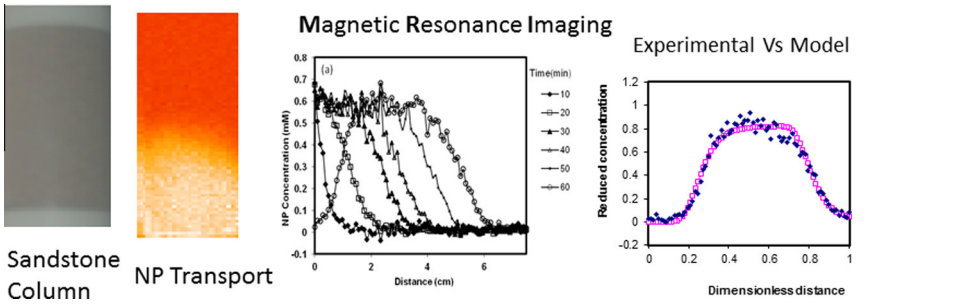

ARTICLE INFO

Article history:
Received 30 October 2014
Received in revised form 11 December 2014
Accepted 18 December 2014
Available online 29 December 2014

Keywords:
Porous media
Nanoparticle transport
Magnetic resonance imaging
CXTFIT model
Environment

ABSTRACT

Transport study of nanoparticle (NP) through matrix flow dominated aquifer sand and soils have significant influence in natural systems. To quantify the transport behaviour, magnetic resonance imaging (MRI) was used to image the iron oxide based nanoparticle, *Molday ION* (carboxyl terminated) through saturated sandstone rock core. T_2-weighted images were acquired and the changes in image intensity were calibrated to get a quantitative concentration profiles at various time intervals. These profiles were evaluated through CXTFIT transport model to estimate the transport parameters. These parameters are estimated at various points along the length of the column while classical breakthrough curve analysis cannot provide these details. NP–surface interactions were investigated using DLVO (Derjaguin–Landau–Verwey–Overbeek) theory. The dispersion coefficients ($2.55–1.21 \times 10^{-7}$ m^2/s) were found to be decrease with distance, deposition rate constant k ($6.70–9.13 \times 10^{-4}$ (1/s)) and fast deposition rate constant k^{fast} ($4.32–8.79 \times 10^{-2}$ (1/s)) were found to be increase with distance. These parameter variations over length will have a scaling up impact in developing transport models for environmental remediation and risk assessment schemes.

1. Introduction

Nanotechnology and nanoparticles (NPs) which are defined as less than 100 nm in length in at least one dimension, is a relatively recent research field that is expanding and diversifying rapidly. NPs have already been utilized in a in a diverse range of applications including textiles, agro-chemicals, electronics, cosmetics, new materials and environmental remediation [1] and the list is expanding. NPs released into environment that moves to ground water and surface water through soil layers can be hazardous to humans and the environment [2]. There is very limited knowledge about the movement and fate of the fast growing engineered nanoparticles, especially when they are released into the ecosystems of environment.

* Corresponding author at: Department of Chemical Engineering & Biotechnology, University of Cambridge, UK.
E-mail address: susithra02@gmail.com (S. Lakshmanan).

http://dx.doi.org/10.1016/j.cej.2014.12.076
1385-8947/

In contrast to the unintentional release of manufactured NPs, nanoparticles are also being designed for in situ remediation of groundwater pollutants, such as polyaromatic hydrocarbons, polychlorinated biphenyls, pesticides, heavy metals [3]. In these cases bespoke nanoparticles, such as zerovalent iron, are injected direct into the groundwater. However, this technology is still in its infancy and their transport behaviour and thus their ability to be delivered to the site of pollution, is still poorly understood [3]. These studies underline the risks associated with nanoparticles to environment and living organisms including humans. Hence accurate data on transport behaviours of NPs in such systems are important in order to design effective remediation strategies.

A number of studies have been carried out to investigate the transport of NPs through water-saturated porous media. Often packed column studies are used to represent the aquifer system. In these conventional methods, the concentration of NPs is calculated from the breakthrough-curve measurement at the column outflow and the data generated is one-dimensional. Even though these experiments provide valuable data on NP transport using colloid filtration theory (CFT), they often fail to predict the transport measurements [4]. In addition, these column tests do not allow the direct observation of local processes [5]. Some of them used this approach to evaluate the deposition by destructively opening packed columns after fixed time intervals [6–8] and often it could disrupt the local flow field or alter the column chemistry [9]. Natural systems (e.g. aquifers and soils) are highly complex and it is important to determine the spatial variability inside packed columns. Changes in particle deposition can occur along the length of the column [10] and these methods could not provide these details. In order to overcome this, non-invasive techniques are required to view the transport processes.

A range of non-invasive methods have been developed such as fluorescent imaging, gamma radiation and X-ray microtomograph. However, there are certain limitations to each of the above mentioned methods. Fluorescent imaging protocols have difficulty in imaging the tracking of fluorescent particles through a translucent packed sand bed [11]. This is due to the dependence of the number of photon penetration and hence the opaqueness of the gravels cannot be investigated. This issue can be overcome by using a scanning optical fibre fluorescence profiler to measure the 2D transport profile. The presence of buried sensors and fibres inside the columns could disturb the transport pathways [12]. Gamma radiation and X-ray micro tomography are widely used for porous media characterization [13], fluid distribution [14] and solute–fluid transport [15] experiments. A major shortcoming of this method is at a single location it requires relatively large counting times and total counting times could be varied between several hours up to one day to produce an image.

Another promising non-invasive technique is magnetic resonance imaging (MRI). Although MRI is mainly used in medical sciences, this technique has already been used in contaminant hydrology research to evaluate colloid transport mechanisms [16], sediment deposition [17], tracer transport through the sediment bed [18] and for investigating transport processes of heavy metals ions such as Gd^{3+}, Cr^{3+} and Cu^{2+} in a sandy aquifer matrix [19]. This method also has a strong potential to quantitatively image the transport of paramagnetic tagged molecules and particles. The transport of paramagnetic colloids through a matrix of silica gel was studied using this method and the spatially resolved data were analysed using the CXTFIT software and colloid filtration theory to predict the behaviour of colloids [20]. Recently the concentration of nanoparticles in a coarse grain system is quantified using this imaging technique [21] and the transport profiles were fitted simultaneously to produce a single set of transport parameters.

Here, we report the transport of NPs in a finer grained system and the transport parameters were estimated individually at various time intervals along the column. In this contribution, we aimed to study the transport of commercially available iron oxide based MRI compatible NP, negatively charged *Molday ION* (*carboxyl terminated*) was used. This is commercially available superparamagnetic iron oxide based NP and 35 nm in diameter and composed of an iron-oxide core surrounded by an organic polymer coating (0.1 mM Fe is equivalent to $\sim 5 \times 10^{15}$ particles/l). Bentheimer sandstone rock core is used to mimic the column test with sandy aquifer. Concentration profiles were analysed with CXTFIT software to estimate transport parameters. Particle–surface interactions were investigated using DLVO theory.

2. Materials and methods

2.1. Porous column and transport experiments

The experiments were performed on Bentheimer sandstone rock core (containing finer quartz grains). The rock core diameter is 37 mm and 75 mm long. Quartz grains are negatively charged at experimental pH conditions [30]. This core was encased in a silicone rubber tube to provide a confining system. This rubber tube has an internal diameter of 35 mm and the wall thickness is 3 mm (Fig. 1). Inlet end caps were used around the ends to make a water tight seal. The column was saturated with water prior to the experiment. The porosity of 0.23 was determined from the weight of the column before and after saturation with water.

The saturated sandstone column was placed horizontally inside a 72 mm diameter bird-cage RF coil at the centre of the MRI bore. All the tubing connected to and from the column was made of PVC. The flow was established by a flow rate of 0.2 ml/min using a HPLC pump (Agilent 1100 Series) using deionised water. An inlet solution of 0.7 mM of *Carboxyl* NP was first pumped into the sandstone column for approximately 50 min. In order to record the NP transport, MR imaging was performed every 5 min. Deionised water was then pumped through for approximately 60 min and the movement of NP transport was imaged.

The presence of NP causes a concentration dependent in T_2. This NP concentration is determined by the following expression [22]:

$$[C] = \frac{1}{R}\left[\frac{1}{T_{2,i}} - \frac{1}{T_{2,0}}\right] \quad (1)$$

where $T_{2,0}$ is the relaxation time in the absence of NP, $T_{2,i}$ is the relaxation time in the presence of NP, $[C]$ is the concentration of the NP, and R is the relaxivity constant of the NP.

2.2. MR imaging

The MR imaging experiments were performed on a *Bruker Avance BioSpec* system, using a 30 cm horizontal bore, 7T superconducting magnet (*Bruker BioSpin*, *Karlsruhe*, *Germany*). A *Bruker*

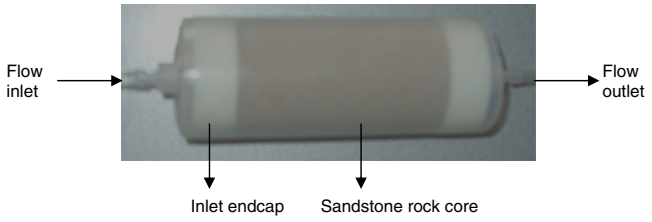

Fig. 1. Photograph of the experimented porous column.

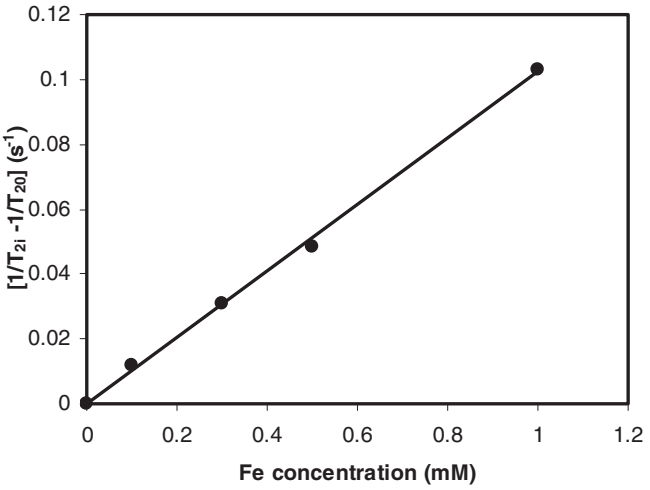

Fig. 2. Variation in the change of transverse relaxation rate with respect to NP concentration.

micro-imaging gradient insert (model BG-6) and 200-A gradient amplifiers were used to provide strong linear magnetic field gradient pulses of up to 1000 mT/m, thus allowing the system to perform micro-imaging experiments. Further technical details of MR imaging can be found in Phoenix et al. [22].

NP transport imaging was performed using a Rapid Acquisition Relaxation Enhanced (RARE) Sequence. The experiments were performed with the following imaging parameters: echo time (T_E) 22 ms, repetition time (T_R) 5000 ms with a RARE factor of 8, field of view was 8.1 cm × 4.5 cm, imaging matrix was 108 × 60 pixels, giving an in-plane resolution of 750 μm with a slice thickness of 3 mm. The imaging time was approximately 3 min. To obtain comparable T_2-weighted images these imaging parameters were kept identical during the entire experiment.

During the NP transport experiment, MR imaging was used to acquire spatially and temporally resolved T_2-weighted images of the column. T_2 is the spin–spin relaxation time of ^{1}H nuclei of the water phase. T_2-weighted images acquired before and after introducing NP can be used to quantify the NP concentration.

2.3. Quantitative measurement of NP concentration

The signal decay at a particular concentration C is obtained using a Rapid acquisition Relaxation Enhancement pulse sequence (RARE) and it is represented by [23]:

$$\frac{S}{S_0} = \exp\left(\frac{-t_e}{T_{2,i}}\right) \tag{2}$$

where S is the MRI signal, S_0 is the signal at zero echo time and T_2 is the spin–spin relaxation time. The effective echo time t_e was chosen to maximize the signal contrast as described in von der Schulenburg et al. [24] and was determined to be 22 ms.

Combining Eqs. (1) and (2) gives the following equation:

$$C = \left[\left(\ln\left(\frac{S}{S_0}\right)\Big/ - t_e\right) - \left(\frac{1}{T_{2,0}}\right)\right]\frac{1}{R} \tag{3}$$

A RARE image of the sample containing only water was appropriately scaled, to get a maximum signal intensity map of S_0. Hence, NP concentrations can be calculated from Eq. (3), using T_2-weighted images acquired before and after introduction of NP.

2.4. Transport parameters estimation

Transport parameters are estimated by using the CXTFIT model and the analytic solutions of the linear convection–dispersion equation (CDE) with a first-order loss term in the model is [25]:

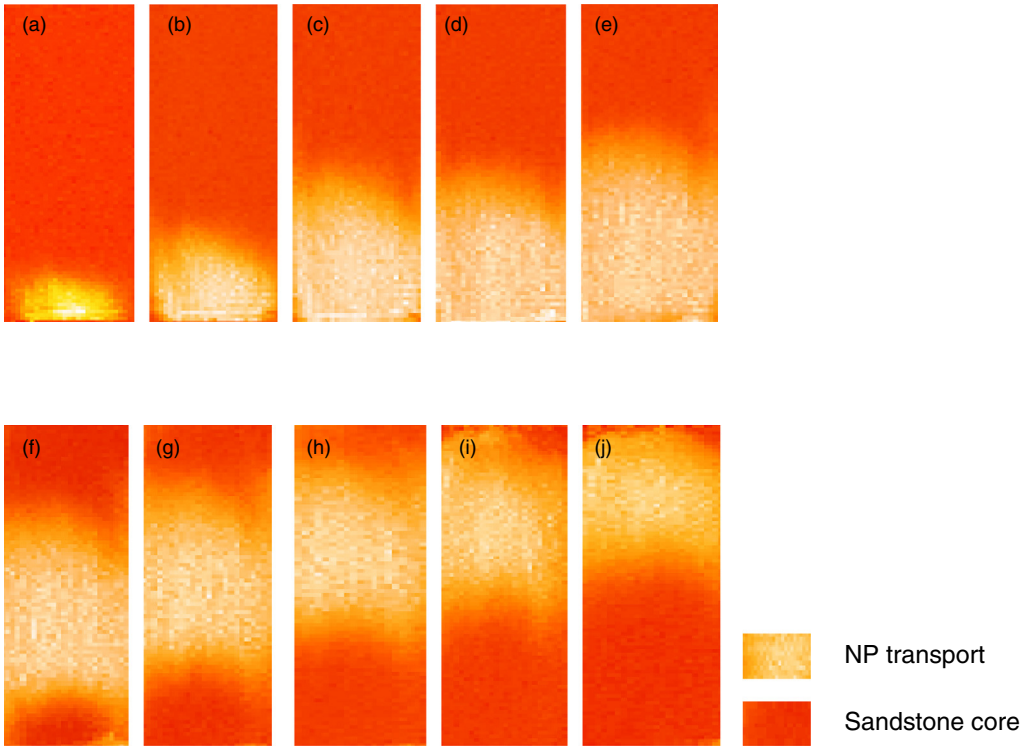

Fig. 3. Calibrated concentration images of *Carboxyl* NP transport inside the sandstone core at 10 min time interval. (a)–(e) NP transport and (f)–(g) movement of NP transport (red in colour region represents the rock core and brighter region represents NP transport). (For interpretation of the references to colour in this figure legend, the reader is referred to the web version of this article.)

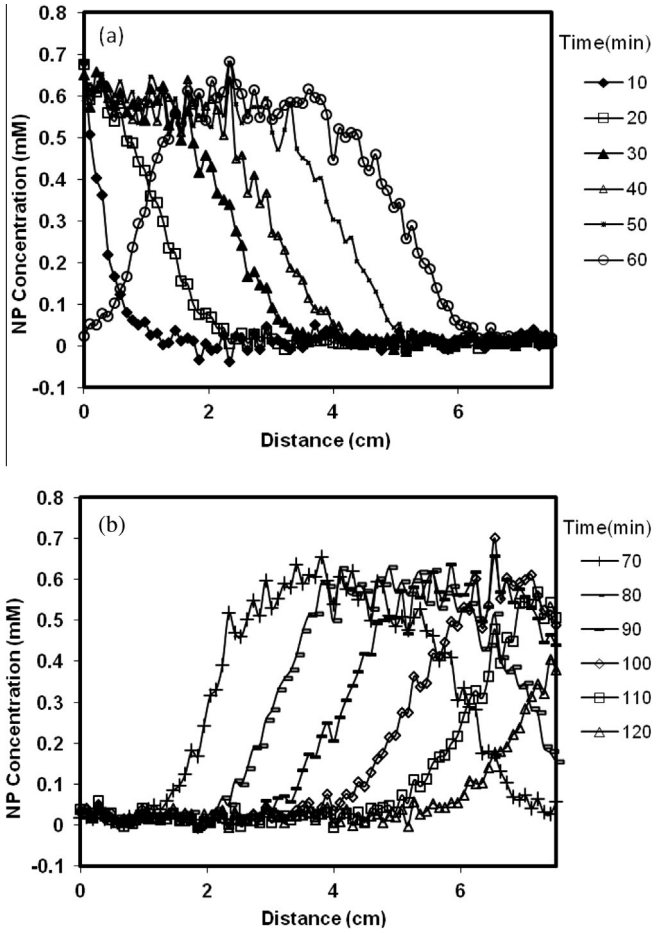

Fig. 4. Concentration profiles of *Carboxyl* NP transport along the flow direction; (a) up to 60 min (b) second half from 70 to 120 min.

$$\frac{\partial C}{\partial t} = D\frac{\partial^2 C}{\partial x^2} - v_p\frac{\partial C}{\partial x} - kC \tag{4}$$

where C is the concentration, t is time, x is distance from the inlet, v_p average particle velocity, D dispersion coefficient and k is the decay coefficient. This solution is encoded in CXTFIT-Excel [26]. The model parameters, D, v_p and k that give the best-fit, measured by the least-square error between modelled and observed concentration profiles were determined using CXTFIT-Excel computer package by Tang et al. [27]. From the estimates of k and the knowledge of the characteristics of the gravel it is possible to gain further insights into the mechanism using colloidal filtration theory.

Colloidal filtration theory is widely applied to characterize the NP interaction to the grain surface, especially estimating particle deposition. Under some limiting assumption [28], the deposition rate can be equated to the decay rate in Eq. (4) and this is expressed as:

$$k = k^{fast}\alpha \tag{5}$$

where k^{fast} is the deposition rate that would occur if all particles that come into contact with grains stick and the sticking efficiency α represents the fraction of NP that remain attached after the collision. The determined form of k^{fast} is the following:

$$k^{fast} = \frac{3(1-\varepsilon)}{2d_c}\eta v_p \tag{6}$$

here ε is the porosity, d_c is the spherical collector diameter and η is the frequency of NP collisions with the porous medium grain surfaces and can be calculated by [28,29]:

$$\eta = 2.4A_s^{1/3}N_R^{-0.081}N_{Pe}^{-0.715}N_{vdw}^{0.052} + 0.55A_sN_R^{1.675}N_A^{0.125} + 0.22N_R^{-0.24}N_G^{1.11}N_{vdw}^{0.053} \tag{7}$$

here A_s a constant specific to the porous medium and it is defined as:

$$A_s = \frac{2(1-\gamma^5)}{(2-3\gamma+3\gamma^5-2\gamma^6)} \tag{8}$$

where $\gamma = \sqrt[3]{1-\varepsilon}$; N_R is the aspect ratio $=\frac{d_p}{d_g}$ where d_p and d_g denote the diameter of the particles and grains, the Peclet number N_{Pe}, the van der Walls number N_{vdw}, N_G is the gravity number and the attraction number N_A is the ratio of $(N_{vdw}/N_{Pe}\cdot N_R)$.

3. Results and discussion

3.1. Determination of the relaxivity constant

In order to measure the relaxivity constant, five different NP concentrations were prepared and each one was injected through a saturated sandstone core, similar to the one used for the transport experiment. T_2 measurement for each sample was recorded with MR Imaging and using the calibration expression (Eq. (1)), relaxation rate $(1/T_{2i} - 1/T_{20})$ has a linear relationship with the concentration and this is shown in Fig. 2.

From the slope of Fig. 2, the relaxivity constant R for the *Carboxyl* NP was determined by the least square fit method to be 123 $mM^{-1}\,s^{-1}$.

3.2. MRI measurements of NP transport through sandstone core

A series of T_2-weighted images were recorded for the transport of *Carboxyl* NP into the sandstone with a time interval of 5 min. These images were calibrated to produce quantitative concentration maps by using Eq. (4). NP transport at 10 min time interval are shown in Fig. 3(a)–(e). After 50 min of NP transport, deionised water was then pumped through for approximately 60 min to capture the NP transport movement. These images are shown are shown in Fig. 3(f)–(j) at 10 min time interval. During the experiment, the transport of NP shortens the T_2 values and this is shown by the increase in measured MRI signal.

All the data was obtained from a 2-D slice through the centre of the column using rapid acquisition sequence. This is desirable for the interpretation of the data analysis and estimating the transport properties. The averaged *Carboxyl* NP concentrations along the column width at 10 min time interval are shown in Fig. 4 and it reaches the sandstone column outlet at 130 min.

3.3. NP transport modelling

The experimental results from the sandstone column are modelled with CXTFIT software. The transport parameters can be estimated at any point along the length of column. The experimental data set from 60 to 80 min gives full transport profiles and concentration profiles at 60, 65, 70 and 75 min are chosen for the analysis.

Concentration profiles at 60, 65, 70 and 75 min are chosen for the analysis. The concentration profiles and the corresponding CXTFIT model data are shown in Fig. 5.

From the graphs we can see that model profiles are largely coinciding with the experimental data, giving goodness-of-fit values (R^2) from 95% to 99%. The fitted transport parameters D, v_p and k are obtained through the CXTFIT model. Fast deposition rate constant k^{fast}, the non-permanent attachment rate is calculated from Eq. (6) and the Sticking efficiency factor α is calculated through Eq. (5). The fitted and derived transport parameters with 95% confidence interval are summarized in Table 1. The averaged disper-

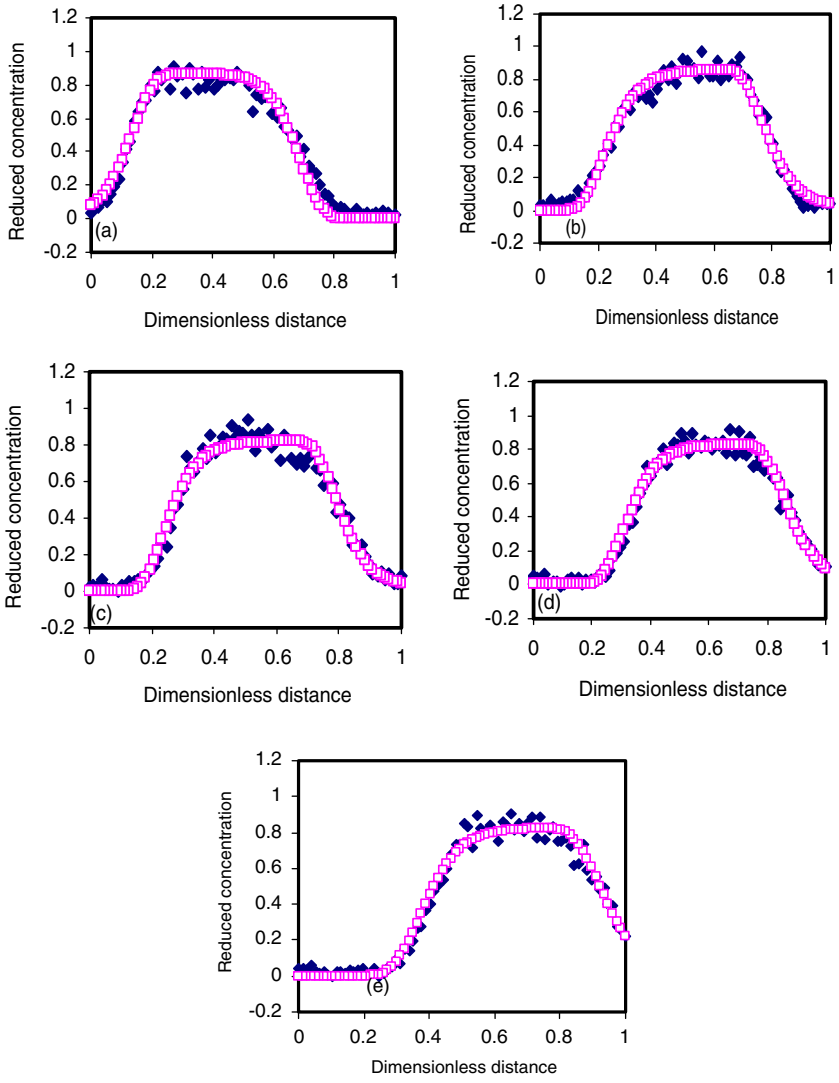

Fig. 5. *Carboxyl* NP concentration profiles at (a) 60 min (b) 65 min (c) 70 min, (d) 75 min (e) 80 min. Closed symbol represents experimental data, and open symbols represent model data.

Table 1
Transport parameters for Rock core experiment using CXTFIT.

Time intervals	D (m^2/s)	v_p (m/s)	k (1/s)	k^{fast} (1/s)	α
60	2.55E−07	2.23E−04	6.70E−04	4.32E−02	0.0133
65	2.19E−07	2.90E−04	7.32E−04	5.63E−02	0.011
70	2.12E−07	3.82E−04	9.36E−04	7.40E−02	0.0108
75	1.53E−07	4.32E−04	9.30E−04	8.38E−02	0.095
80	1.21E−07	4.53E−04	9.13E−04	8.79E−02	0.089

sion coefficient D_{ave} is 1.92×10^{-7} m^2/s. Khrapitchev and Callaghan [31] reported the relationship between the dispersion coefficient and the porous media characteristics for various literature studies. Their relationship gives a D_{ave} value of 1.52×10^{-7} m^2/s which is same order of magnitude. This supporting the robustness of the MRI approach, in quantifying NP transport. During the progress of NP plume, almost constant dispersion coefficient achieved for the first three profiles which is in between 2.55 and 2.12×10^{-7} m^2/s and then starting to have a drop by factor of 0.60 for the subsequent data sets.

The other derived parameters also showed some variation; v_p increased by a factor of ~0.5 over the time and distance. This could be due to the heterogeneity in NP characteristics, finer grain systems and column length.

Fast deposition rate constant k^{fast} is in the range of $4.32 - 8.79 \times 10^{-2}$ (1/s). The rate constant k is known as permanent attachment rate and it is in the range of $6.70 - 9.13 \times 10^{-4}$ (1/s). The calculated sticking efficiency factor α was found to be less variation till 70 min and then it varies from 0.013 to 0.09. Earlier literature suggests [32] that some deposition could occur in secondary energy minima between the same surface charge NP and the porous medium. As we have seen in the analysis, certain amount of deposition is observed as a measure of deposition rate constants (k and k^{fast}). NP–grain surface interactions and the interaction energy profiles including secondary energy minima usually described by DLVO theory and derivatives. The following section explores this deposition behaviour using this classical DLVO theory.

3.4. DLVO interaction energy profiles

Particle deposition behaviour is classified as favourable and unfavourable interactions [32]. When the particle and collector have similar surface charge, the interactions are classified as unfavourable and the deposition can occur in secondary energy minima

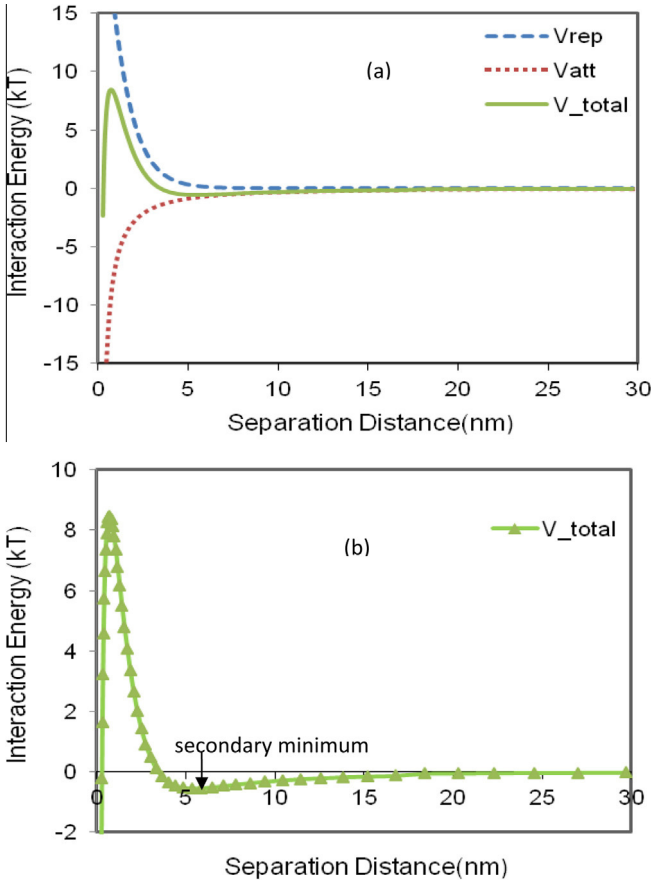

Fig. 6. (a) Interaction energy profile generated with DLVO theory, (b) re plot for total energy profile.

[33]. The deposition behaviour for nanoparticle and colloids are reported in the literature [34]. Interaction energy profiles are estimated using DLVO theory [35,36]. The total interaction potential is the sum of electrostatic repulsion (V_{rep}) and the attractive potential (V_{att}) and it was determined for the NP–sandstone core by treating as a sphere–plate interaction. V_{rep} and V_{att} were calculated using the expression of Hogg et al. [37] and Gregory [38]. Zeta potential value for sand grain was taken from the literature [39] and Hamaker constant of 10^{-20} J was used in this analysis [32,40].

DLVO interaction energy profile is shown in Fig. 6(a) and (b). Presence of repulsive energy barrier is observed (unfavourable condition due to the negatively charged surfaces) with secondary energy minima.

In Fig. 6(b), the total interaction energy profile is re plotted on a different scale to measure the energy barrier and the secondary energy minima; the height of energy barrier 8 kT and depth of the secondary energy minimum of 0.55 kT was measured. In the present study, despite little electrostatic attraction between the negatively charged NP and the negatively charged quartz grain, the observed deposition is likely due to deposition of NPs in weak secondary energy minima [33,41] as we observed in the DLVO energy profiles.

4. Conclusion

MRI offers good potential to study particle transport patterns inside packed columns. Transport of *Carboxyl* NP inside water-saturated sandstone core was successfully studied with MRI. The spatially and temporally resolved NP transport data was analysed with CXTFIT to study the transport behaviour. Particle surface interactions were examined with DLVO theory. This study provides valuable information, the key transport parameters such as dispersion coefficient, deposition rate constant and the sticking efficiency were reported. The observed variations in transport parameters over time would not be detectable from standard breakthrough curve analysis. These length dependant variations have significant scaling-up implications for transport models used to predict NP transport in finer grained systems representative of soils and aquifers. Also the benefit of utilizing MR imaging technique, spatially resolved data collection that MRI can provide is highlighted.

Acknowledgements

This research was undertaken with financial support from the Engineering and Physical Sciences Research Council (EP/G028443/1) and Natural Environmental Research Council (NE/G010269/1) at University of Glasgow. We also thank Jim Mullen for his assistance with MRI experiments.

References

[1] L. Zhen, S.D. Endalkachew, A.H. Ashraf, Transport and deposition of CeO_2 nanoparticles in water-saturated porous media, Water Res. 45 (2011) 4409–4418.
[2] J. Seung-Woo, K. Sung-Dong, Aggregation and transport of copper oxide nanoparticles in porous media, J. Environ. Monit. 11 (2009) 1595–1600.
[3] B. Karn, T. Kuiken, M. Otto, Nanotechnology and in situ remediation: a review of the benefits and potential risks, Environ. Health Perspect. 117 (2009) 1823–1831.
[4] C.C. Choy, M. Wazne, X.G. Meng, Application of an empirical transport model to simulate retention of nanocrystalline titanium dioxide in sand columns, Chemosphere 71 (2008) 1794–1801.
[5] N. Nikolaus, W. Arthur, N. Reinhard, B. Thomas, Spatial and temporal observations of adsorption and remobilization of heavy metals ions in a sandy aquifer matrix using MRI, Environ. Sci. Technol. 37 (2003) 3972–3977.
[6] R.W. Puls, R.M. Powell, Transport of inorganic colloids through natural aquifer material: implications for contaminant transport, Environ. Sci. Technol. 26 (1992) 614–621.
[7] S.A. Bradford, S.R. Yates, M. Bettahar, Simunek, Physical factors affecting the transport and fate of colloids in saturated porous media, J. Water Resour. Res. 38 (2002) 1327.
[8] S.A. Bradford, J. Simunek, M. Bettahar, M.T. van Genuchten, S.R. Yates, Modelling colloid attachment, straining and exclusion in saturated porous media, Environ. Sci. Technol. 37 (2003) 2242–2250.
[9] T. Baumann, C.J. Werth, Visualization of colloid transport through heterogeneous porous media using magnetic resonance imaging, Colloids Surf. A: Physicochem. Eng. Aspects 265 (2005) 2–10.
[10] H.F. Lecoanet, M.R. Wiesner, Velocity effects on fullerene and oxide nanoparticle deposition in porous media, Environ. Sci. Technol. 38 (2004) 4377.
[11] J.W. Bridge, S.A. Banwart, A.L. Heathwaite, Noninvasive quantitative measurement of colloid transport in mesoscale porous media using time lapse fluorescence imaging, Environ. Sci. Technol. 40 (2006) 5930–5936.
[12] J. Shang, C. Liu, Z. Wang, H. Wu, K. Zhu, J. Li, Liu, In-situ measurements of engineered nanoporous particle transport in saturated porous media, J. Environ. Sci. Technol. 44 (2010) 8190–8195.
[13] T.H. Illangasekare, J.L. Ramsey, K.H. Jensen, M.B. Butts, Experimental study of movement and distribution of dense organic contaminants in heterogeneous aquifers, J. Contam. Hydrol. 20 (1995) 1–25.
[14] M.L. Brusseau, H. Janousek, A. Murao, G. Schnaar, Synchrotron X-ray microtomography and interfacial partitioning tracer test measurements of NAPL–water interfacial areas, Water Resour. Res. 44 (2008) 1–9.
[15] C. Hofstee, M. Oostrom, J.H. Dane, R.W. Walker, Infiltration and redistribution of perchloroethylene in partially saturated stratified porous media, J. Contam. Hydrol. 34 (1998) 293–313.
[16] J.W. Charles, Z. Changyong, L.B. Mark, O. Mart, A. Thomas Baumann, A review of non-invasive imaging methods and applications in contaminant hydrogeology research, J. Contam. Hydrol. 113 (2010) 1–24.
[17] H. Heather, V. Elisa, H. William, Using magnetic resonance imaging for experimental analysis of fine-sediment infiltration into gravel beds, Sedimentology 56 (2009) 1961–1975.
[18] L. Susithra, P. Gareth, H. Heather, H. William, Characterization of flow transport within pore spaces of an open-work gravel bed, Int. J. Eng. Technol. 3 (2014) 457–463.
[19] N. Nestle, A. Wunderlich, R. Niessner, T. Baumann, Spatial and temporal observations of adsorption and remobilization of heavy metal ions in a sandy aquifer matrix using magnetic resonance imaging, Environ. Sci. Technol. 37 (2003) 3972–3977.

[20] T. Baumann, C. Werth, Visualization of colloid transport through heterogeneous porous media using magnetic resonance imaging, J. Colloids Surf. A: Physicochem. Eng. Aspects 265 (2005) 2–10.
[21] B. Ramanan, M.H. William, T.S. William, R.P. Vernon, Investigation of nanoparticle transport inside coarse-grained geological media using magnetic resonance imaging, Environ. Sci. Technol. 46 (2012) 360–366.
[22] V.R. Phoenix, W.M. Holmes, Magnetic resonance imaging of structure, diffusivity and copper immobilization in a phototrophic biofilm, Appl. Environ. Microbiol. 74 (2008) 4934–4943.
[23] E.M. Haacke, R.W. Brown, M.R. Thompson, R. Venkatesan, Magnetic Resonance Imaging: Physical Principles and Sequence Design, Wiley-Liss, 1999.
[24] D.A. Graf vonder Schulenburg, D.J. Holland, M. Paterson-Beedle, L.E. Macaskie, L.F. Gladden, M.L. Johns, Spatially resolved quantification of metal ion concentration in a biofilm-mediated ion exchanger, Biotechnol. Bioeng. 99 (2008) 821.
[25] J.M. Wraith, D. Or, Non linear parameter estimation using spreadsheet software, J. Nat. Resour. Life Sci. Educ. 27 (1998) 13.
[26] N. Toride, F.J. Leij, M.Th. van Genuchten, The CXTFIT Code for Estimating Transport Parameters from Laboratory or Field Tracer Experiments, 1995. Version 2.0, Research Report No. 137, U.S. Salinity Laboratory, USDA, ARS, Riverside, CA.
[27] G. Tang, M.A. Mayes, J.C. Parker, P.M. Jardine, CXTFIT/Excel – a modular adaptable code for parameter estimation, sensitivity analysis and uncertainty analysis for laboratory or field tracer experiments, Comp. Geosci. 36 (2010) 1200.
[28] K.M. Yao, M.T. Habibian, C.R. OMelia, Water and waste water filtration. Concepts and applications, Environ. Sci. Technol. 5 (1971) 1105–1112.
[29] N. Tufenkji, M. Elimelech, Correlation equation for predicting single-collector efficiency in physicochemical filtration in saturated porous media, Environ. Sci. Technol. 38 (2004) 529–536.
[30] J. Yu, J.M. Berlin, Transport study of nanoparticles for oilfield application, vol. 10, in: SPE International Conference on Oilfield Scale, Aberdeen, UK, 2010, pp. 512–528.
[31] A.A. Khrapitche, P.T. Callaghan, Reversible and irreversible dispersion in a porous medium, Phys. Fluids 15 (2003) 2649.
[32] M. Elimelech, C.R. O'Meilat, Kinetics of deposition of colloidal particles in porous media, Environ. Sci. Technol. 24 (1990) 1528–1536.
[33] M. Hahn, D. Abadzic, et al., Aquasols: on the role of secondary minima, Environ. Sci. Technol. 38 (2004) 5915–5924.
[34] N. Tufenkji, M. Elimelech, Breakdown of colloid filtration theory: role of the secondary energy minimum and surface charge heterogeneities, Langmuir 21 (2005) 841–852.
[35] B.V. Derjaguin, L.D. Landau, Theory of the stability of strongly charged lyophobic sols and of the adhesion of strongly charged particles in solutions of electrolytes, Acta Physicochim. USSR 14 (1941) 733–762.
[36] E.J.W. Verwey, J.Th.G. Overbeek, Theory of the Stability of Lyophobic Colloids, Elsevier, Amsterdam, 1948.
[37] R. Hogg, T.W. Healy, D.W. Fuerstenau, Mutual coagulation of colloidal dispersions, Trans. Faraday Soc. 62 (1966) 1638–1652.
[38] Gregory, Approximate expressions for retarded van der waals interaction, J. Colloid. Interface Sci. 83 (1981) 138–145.
[39] C.M. Cerda, K. Non-Chhom, The use of sinusoidal streaming flow measurements to determine the electrokinetic properties of porous media, Colloids Surf. 35 (1989) 7–15.
[40] I. Chowdhury, Y. Hong, et al., Mechanisms of TiO_2 nanoparticle transport in porous media: role of solution chemistry, nanoparticle concentration, and flow rate, J. Colloid Interface Sci. 360 (2011) 548–555.
[41] A. Petosa, D.P. Jaisi, et al., Aggregation and deposition of engineered nanomaterials in aquatic environments: role of physicochemical interactions, Environ. Sci. Technol. 44 (2010) 6532–8549.